Characterization of a Poly-4-Vinylpyridine-Supported CuPd Bimetallic Catalyst for Sonogashira Coupling Reactions

Claudio Evangelisti,*[a] Antonella Balerna,*[b] Rinaldo Psaro,[a] Graziano Fusini,[a, c] Adriano Carpita,[c] and Maurizio Benfatto[b]

CuPd bimetallic solvated metal atoms (SMA) synthesized by metal vapor synthesis (MVS) technique and supported on poly-4-vinylpyridine (PVPy) resin, showed significantly higher catalytic activity in Sonogashira-type carbon–carbon coupling reactions than the corresponding monometallic Cu and Pd systems as well as their physical mixture. The analysis of the bimetallic catalyst combining transmission electron microscopy techniques and X-ray absorption fine structure (XAFS) spectroscopy revealed the presence of small Pd nanoparticles ($d_m = 2.5$ nm) while the analysis of the X-ray absorption data, at the Cu K-edge suggests the formation of thin and incomplete Cu oxide layers around the Pd-rich cores.

1. Introduction

Bimetallic systems, thanks to their catalytic, electronic and optical properties, are of great interest from both a scientific and an industrial point of view.[1–4] The catalytic properties of these systems are greatly influenced by the size and shape of their particles, similar to monometallic systems, as well as by their chemical states and the distribution of the two metals within the individual nanoparticles (e.g. alloying, core–shell structure, or segregation).[5–8]

Supported bimetallic nanoparticles (NPs) deriving from a combination of group VIII atoms (e.g. Pd) and group IB ones (e.g. Cu) have been extensively studied in different chemical catalytic processes such as the reduction of nitrates and nitrites,[9,10] hydrogenation reactions,[11,12] CO[13] or volatile organic compounds (VOCs)[14] catalytic oxidations, and the electrochemical oxidation of methanol.[15] Theoretical studies demonstrated that the marked electron donor character of Cu, in CuPd NPs, modifies the electronic properties of Pd, which acts as an acceptor, by lowering the Pd d-band and injecting electronic charge in the 5sp-one.[16,17] Recently, the presence of Cu in CuPd NPs proved to significantly enhance the catalytic performances of Pd catalysts in carbon–carbon coupling reactions (e.g. Suzuki–Miyaura and Sonogashira reactions) allowing the development of new CuPd catalysts that require also a reduced amount of precious Pd metal.[18–31]

The cross-coupling of a sp^2-carbon of an aryl or vinyl halide with a terminal *sp* hybridized carbon from an alkyne, commonly termed as Sonogashira reaction, is one of the most powerful tools to prepare important precursors of natural products, agrochemicals and pharmaceuticals, as well as molecular materials (optical or electronic) .[32–36] Homogeneous palladium salts or organometallic complexes with an excess of phosphine ligands together with copper(I) species are commonly used as catalysts to facilitate the coupling through the transmetallation of alkynes.[36] On the other hand, the development of supported catalysts is a promising way to ensure an easy separation and reusability of the catalytic systems, avoiding environmental pollution coming from heavy metallic ions.[32]

Herein, we report the synthesis of a CuPd bimetallic catalyst derived from Cu and Pd vapors, according to the metal vapor synthesis (MVS) technique, and supported on a commercially available poly-4-vinylpyridine cross-linked with divinylbenzene (PVPy) resin.[37]

The CuPd/PVPy system showed a high catalytic activity in the Sonogashira reaction of iodobenzene with phenylacetylene carried out with a molar ratio iodide/Pd = 1000 at 95 °C in air atmosphere, resulting in 100% conversion after 2.5 h (specific activity, SA = 520 h^{-1}).[38] The catalytic efficiency of CuPd/PVPy was higher than previously reported supported CuPd bimetallic systems,[22–26] taking also into account the low doses employed. Moreover, thanks to the coordinative capability the PVPy support, the amounts of metals leached by the CuPd/PVPy system were very low (0.6 ppm of Pd and 3.0 ppm of Cu in the crude reaction product) with respect to the ones of an analogous system supported on carbon.[38]

In this paper, we show the catalytic performances of the CuPd/PVPy system in Sonogashira coupling reaction of phenylacetylene with 4-iodobenzene compared with those of the analogously prepared Pd or Cu monometallic catalysts (Pd/

[a] *Dr. C. Evangelisti, Dr. R. Psaro, Dr. G. Fusini*
Institute of Molecular Science and Technologies, CNR
via G. Fantoli 16/15, 20138 Milano (Italy)
E-*mail: claudio.evangelisti@istm.cnr.it*
[b] *Dr. A. Balerna, Dr. M. Benfatto*
Frascati National Laboratories, INFN
Via E. Fermi 40, 00044 Frascati, Roma (Italy)
E-*mail: antonella.balerna@inf.infn.it*
[c] *Dr. G. Fusini, Prof. A. Carpita*
Department of Chemistry and Industrial Chemistry, University of Pisa Via G. Moruzzi 13, 56124 Pisa (Italy)

PVPy or Cu/PVPy) and of their equivalent mixture (Pd/PVPy + Cu/PVPy). Results obtained with the bimetallic system in Sonogashira reactions with different (hetero)aryl iodides are also reported.

In order to gain a deeper insight into the relationship between the catalytic efficiency of the CuPd/PVPy system and its structural features, a detailed structural characterization was performed. The size distribution of the nanoparticles and the metal dispersion on the PVPy support were investigated by transmission electron microscopy (TEM) and high-angle annular dark-field scanning transmission electron microscopy (HAADF-STEM) combined with energy dispersive X-ray spectroscopy (EDS) to obtain the Cu and Pd elemental maps. The structural characterization of the catalysts at the Pd K edge was already published[38], whereas we report herein the structure of the Cu atoms in the bimetallic sample by using X-ray absorption spectroscopy (XAFS) at the Cu K-edge. The extended X-ray absorption fine structure (EXAFS) and near edge (XANES) spectra of the bimetallic catalysts and of the reference samples (Cu_2O and CuO bulk oxides and Cu foil) have been taken into account. Structural information concerning the coordination numbers (N) interatomic distances (R) and Debye-Waller factors (σ^2) of the bimetallic sample have been achieved by the EXAFS data analysis and have been confirmed by the fitting procedure applied to the XANES spectrum.

2. Results and Discussion

Transmission electron microscopy (TEM) analysis of the MVS-derived CuPd/PVPy system revealed that the resin was densely populated by metal nanoparticles distributed in a narrow range (1.0 nm–4.5 nm) with a mean diameter (d_m) of about 2.5 nm and a standard deviation (SD) of 0.7 nm (Figure 1). The representative micrograph shows the presence of nanoparticles well embedded in the polymeric resin in agreement with previously reports on the strong affinity of metal nanoparticles with the pyridine moiety of the support.[37] On the other hand, the monometallic Pd/PVPy system synthesized using the same procedure contained metal particles with slightly larger sizes (d_m = 2.9 nm; SD = 1.3 nm) and a broader size distribution (1.0–7.5 nm) (see Figure 2), indicating that the presence of Cu affects the metal atoms aggregation. High resolution TEM and lattice fringe analysis of the PVPy-supported bimetallic catalysts revealed the presence of nanostructured Pd particles having a contracted face cubic centered (fcc) structure.[38] The CuPd/PVPy catalyst showed a high dispersion of the Pd and Cu phases within the PVPy support as evidenced by STEM-EDS elemental maps of a representative catalyst grain reported in Figure 3. The resulting EDS spectrum analysis gave a Pd/Cu molar ratio of 2.2, which is very similar to that revealed by inductively coupled plasma optical emission spectrometry (ICP OES) analysis (Pd/Cu molar ratio 2.0 corresponding to 1.0 wt.% of Pd and 0.3 wt.% of Cu on PVPy).

Like HRTEM, also EXAFS data analysis at the Pd K-edge showed the presence of small fcc Pd nanoparticles having contracted interatomic distances[38, 39] in the case of the bimetallic sample and that both the monometallic and the bimetallic cat-

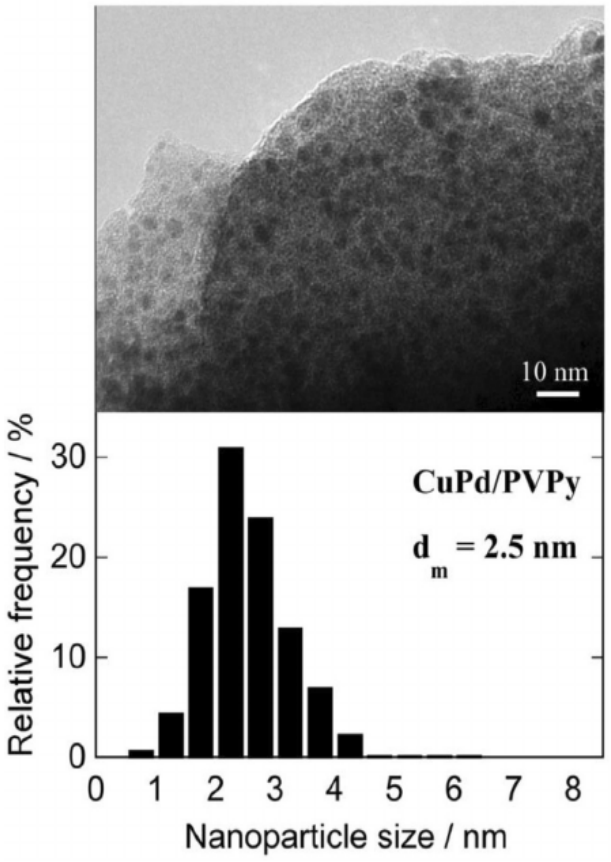

Figure 1. Representative TEM micrograph and nanoparticle size distribution of the bimetallic CuPd/PVPy catalyst.

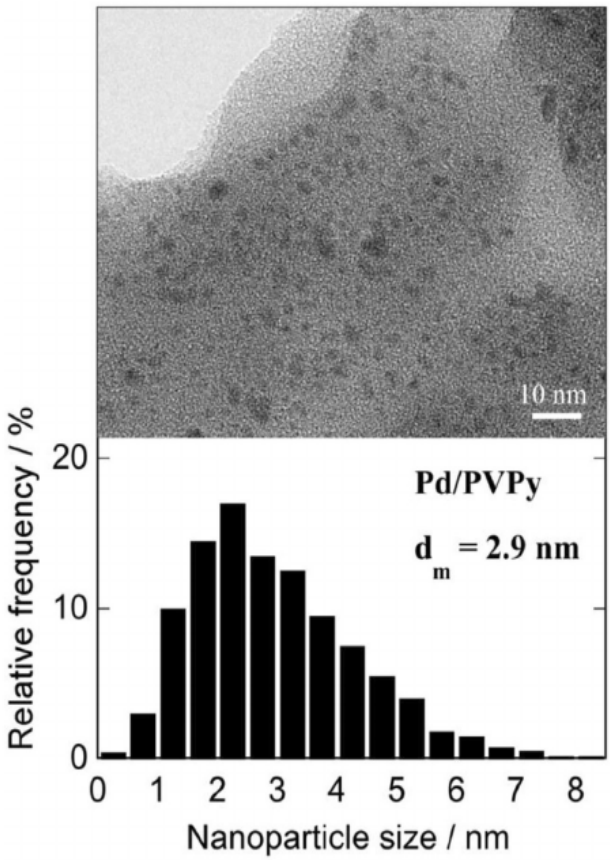

Figure 2. Representative TEM micrograph and nanoparticle size distribution of the monometallic Pd/PVPy catalyst.

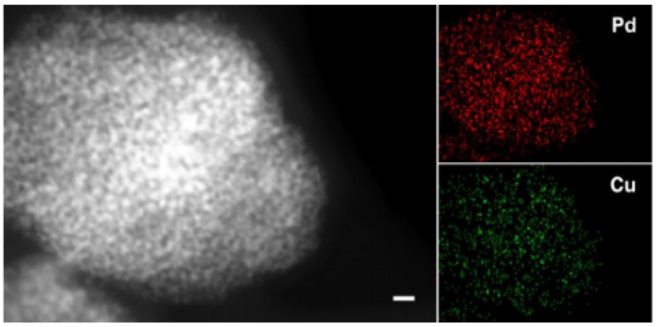

Figure 3. High-angle annular dark-field imaging (HAADF)-STEM image (the length of the bar corresponds to 10 nm) of a grain of the CuPd/PVPy catalyst (left side) and STEM-EDS mapping of the catalyst showing the Pd and Cu dispersion present in the catalyst (right side).

alysts have a first shell Pd–O contribution.[38] As recently found using XPS investigations of MVS-derived samples,[40], Pd atoms are mainly present in a Pd^0 phase, but small amounts can be in a Pd^{2+} one. Owing to the rather small dimensions of the Pd-based nanoparticles, the Pd atoms on the surface of the nanoparticles can be easily oxidized to form thin surface layers of PdO when treated in air atmosphere. It is important to stress that these thin oxide layers do not affect the catalytic properties of the catalysts, because similar results were obtained in Sonogashira reactions carried out both in air and in inert (i.e. argon) atmosphere, as reported below.

The EXAFS data analysis at the Pd K-edge gave also a small Pd–Cu contribution with an interatomic distance, $R = 2.68$ Å.

Concerning the XAFS data analysis, at the Cu K-edge (Figure 4), in the monometallic Cu/PVPy sample, no metallic phase was found.[41] The deposition of monometallic Cu on PVPy resulted in the formation of Cu_2O nanoparticles,[41] as already observed by other authors,[42] with a thin CuO surface layer. The presence of Cu_2O nanoparticles, in the Cu/PVPy monometallic sample, is clearly visible from the position of the peak in the near edge region shown in Figure 4 (dotted line). This single absorption peak is normally assigned to the electric dipole-allowed transitions, characteristic of Cu^{1+} ($3d^{10}$) samples like Cu_2O.[43] As already reported[38] and will be further on confirmed, the Cu/PVPy monometallic system resulted almost inactive in the reaction conditions used for Sonogashira coupling reactions.

The analysis of the bimetallic CuPd/PVPy sample, at the Cu K-edge, was more complex. As reported in Table 1, in this sample there was no presence of a Cu_2O-like structure (see Figure 5). Bulk Cu_2O has a cubic structure with two oxygen atoms as nearest neighbors at a distance of about 1.85 Å.[44] However, the first shell Cu–O distance given by the EXAFS data analysis of the CuPd sample was longer (1.94 Å) and similar to the Cu–O bond distances typical of Cu^{2+} compounds like CuO. CuO has a monoclinic crystal structure with Cu atoms having octahedral distorted oxygen coordination with 4 O atoms at about 1.96 Å in a square-type configuration and two axial O atoms at a quite long distance of about 2.78 Å.[45] Probably due to high Debye–Waller factors and/or interference with other higher coordination shells contributions, even if present, the EXAFS data analysis of bulk CuO does not give this long

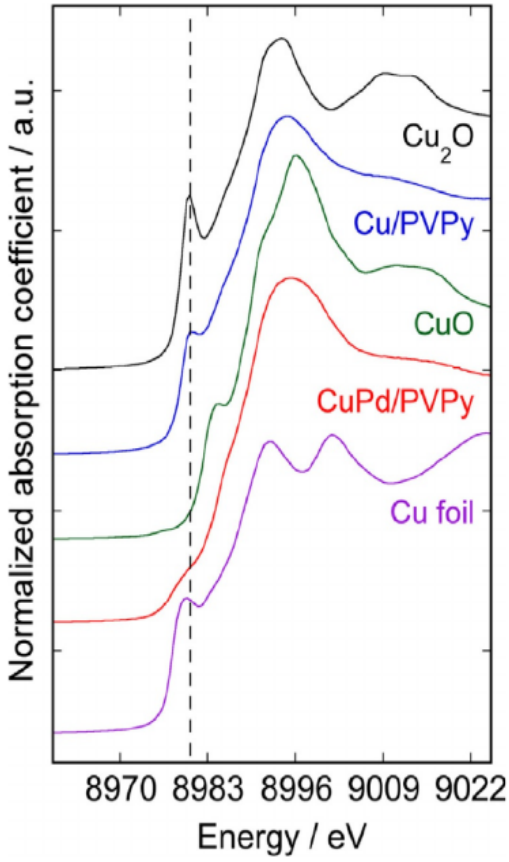

Figure 4. Normalized XANES spectra of the monometallic Cu/PVPy and bimetallic CuPd/PVPy catalysts compared to the ones of the reference samples.

Table 1. Results achieved from the EXAFS data analysis at the Cu K-edge [k^2-weighting and fitting range: (2.7–12.2) $Å^{-1}$].

Sample	Coordination shell	N	R [Å]	σ^2 [$Å^2$]
Cu foil	Cu–Cu 1st shell	12 (fixed)	2.544(7)	0.0044(4)
R-factor = 0.005				
Cu_2O	Cu–O (Cu^{+})	2 (fixed)	1.854(7)	0.0045(4)
R-factor = 0.01	Cu–Cu (Cu^{+})	12 (fixed)	3.024(8)	0.0097(7)
CuO	Cu–O (Cu^{2+})	4 (fixed)	1.955(7)	0.0024(3)
R-factor = 0.004	Cu–Cu (Cu^{+})	4 (fixed)	2.901(8)	0.0035(4)
CuPd/PVPy	Cu–O(Cu^{+})	3.2(4)	1.94(2)	0.0042(4)
R-factor = 0.003	Cu–O(Cu^{+})	1.3(3)	2.52(2)	0.0071(6)
	Cu–Pd	0.8(2)	2.68(2)	0.0084(5)

axial Cu–O distance (see Table 1).[46] The EXAFS data analysis of the CuPd/PVPy sample revealed the presence of two Cu–O coordination shells consistent with Cu^{2+} ions coordinated with O atoms at short (1.94 Å) and longer (2.52 Å) distances and a Cu–Pd contribution exhibiting a distance and coordination number compatible with the results obtained at the Pd K-edge.[38] The two different Cu–O distances found were also confirmed by the presence of the two peaks (labelled C and D) between 8981 eV and 8993 eV in the first derivative of the XANES spectrum of the CuPd sample (Figure 5) that are normally associated to a tetragonal distortion of the CuO_6 octahedron[47–49] that gives shorter equatorial and longer axial Cu–O

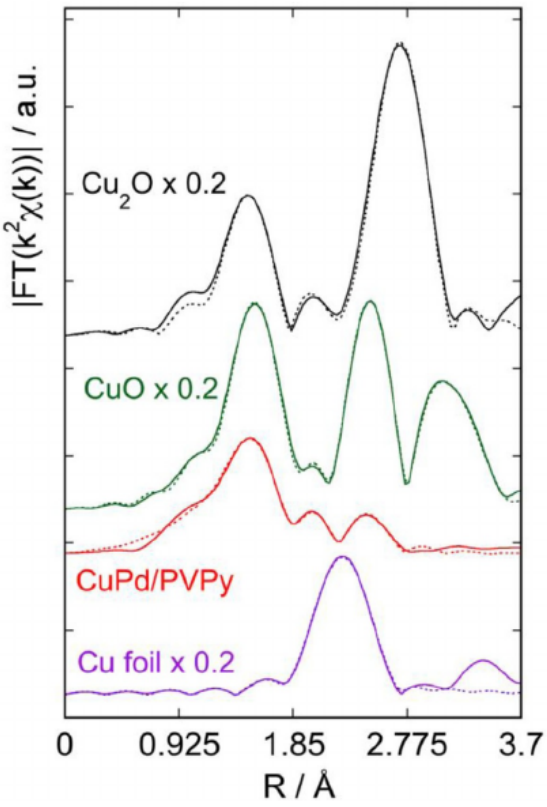

Figure 5. Fourier transforms of the experimental (full lines) and theoretical (dashed lines) EXAFS spectra of the CuPd/PVPy sample compared to the ones of reference samples.

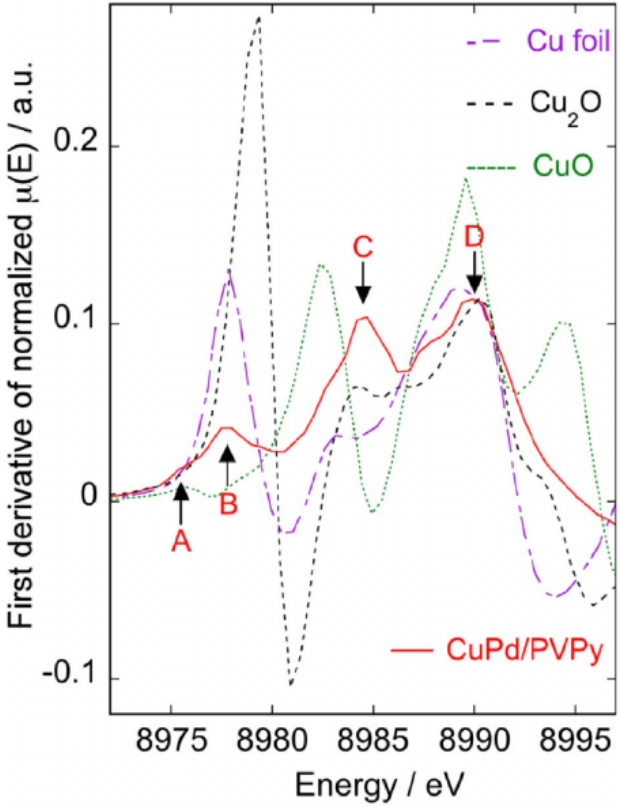

Figure 6. First derivatives of the normalized X-ray absorption spectra, μ(E), of the bimetallic CuPd/PVPy catalyst and of the Cu foil, CuO and Cu_2O reference samples.

bonds. In the absence of a tetragonal distortion, the splitting observed in Figure 6 disappears. When the tetragonal distortion is present, it was shown[47,48] that there also is a relation between the difference of these two distances (the amount of distortion) and the energy separation of the two characteristic features. In our case, we found a distortion or a positive elongation of about 0.58 Å and an energy separation comparable to the value reported in Ref [19].

Cu^{2+} ions have a $3d^9$ electronic configuration and looking at Figure 4, the structure on the rising edge of the CuPd/PVPy XANES spectrum is the convolution of two contributions (energy range 8974 eV–8980 eV),which is better visible in the plot of the first derivative of the near edge region reported in Figure 6. These contributions are a weak pre-edge absorption feature, A, corresponding to a 1s→3d dipole-forbidden but quadrupole-allowed transition,[43] characteristic of Cu^{2+} ($3d^9$) compounds like CuO and a 1s→4p transition contribution, B, indicating a Cu^{2+} reduction: as clearly visible in Table 1, missing a Cu-Cu contribution this B feature could be related to the small Cu-Pd contribution given by the EXAFS data analysis.[50] Taking into account the results achieved by the EXAFS data analysis and a very simple model, using the MXAN[51] program, we tried to reproduce the features B, C and D observed in the first derivative of the XANES spectrum of the bimetallic CuPd sample (see Figure 6). Due to the coordination numbers found, we considered Cu atoms forming thin, defective, and incomplete oxide shells around partially oxidized Pd nanoparticles. Different models have been initially tested using separately six and five fold clusters, but we were not able to reproduce the observed features. Taking into account the coordination numbers given by the EXAFS data analysis and reported in Table 1, we achieved a good fitting (error function value, $R_{sq} = 0.8$) only when two different structural six and five fold sites were included: an octahedron with a tetragonal distortion and a trigonal bi-pyramidal one. The five-fold trigonal bipyramidal site helps taking into account the defective and incomplete oxide shell that can cause a departure from the octahedral coordination.[52] The CuO_6 octahedron included four equatorial O atoms and an axial one treated as free parameters, whereas the other axial one was fixed at the elongated value found (2.52 Å). The trigonal bipyramidal cluster included three equatorial O atoms at a fixed value of 1.95 Å, an axial Pd atom at 2.68 Å (fixed) and an axial O atom taken as free parameter. In both sites, the coordination angles were kept fixed and during the fitting procedures the two sites were continuously and separately optimized until a reasonable convergence was reached. Taking into account the simple model used, the agreement with the experimental XANES spectrum shown in Figure 7 is quite good over the whole energy range used. The XANES analysis confirmed the need to include the Cu–Pd and the elongated Cu–O axial distances.

While in the monometallic Cu/PVPy sample there was the formation of Cu_2O nanoparticles, in the bimetallic one we found the formation of a Cu^{2+} like oxide. The difference be-

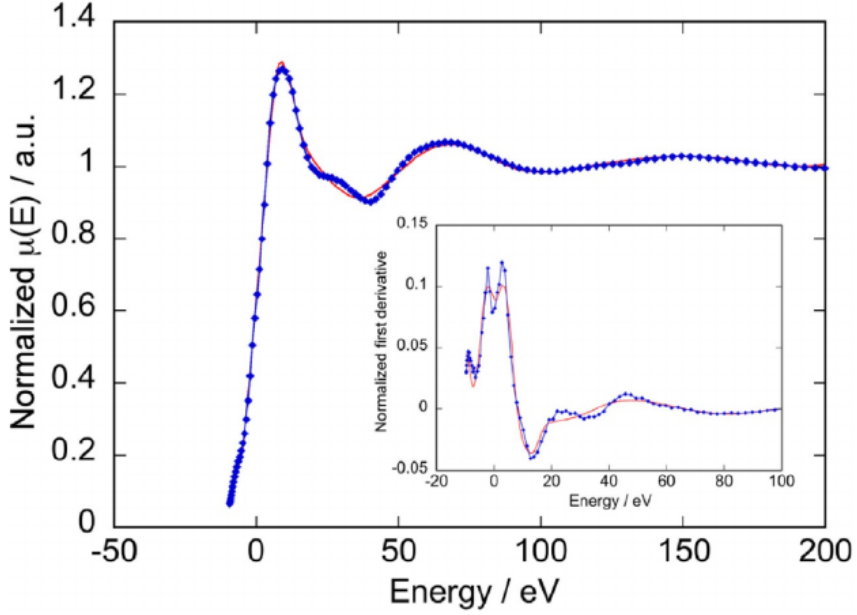

Figure 7. Comparison between the experimental data (dots) and the MXAN fit (continuous line) of the XANES region of the CuPd/PVPy catalyst; in the inset the first derivatives of the experimental near edge data (dots) and of the theoretical ones (full line).

tween the formed oxides in the monometallic and bimetallic samples can probably be related to structural constrains, present in the CuPd/PVPy sample, depending on lattice mismatches between the Pd core and external layer that can influence the stoichiometry of the oxide layer. Probably the large lattice mismatch between cubic Cu_2O and the Pd nanoparticles, that have an f.c.c. structure, favors the formation of the Cu^{2+} like oxide shell and not the Cu_2O one.[53]

Concerning the surface position of the Cu^{2+} ions, the surface segregation of copper in CuPd catalysts[2] is well known. The presence of air surely favors the formation of copper oxide species by the oxidation of the starting Cu^0 atoms and oxidation itself, being energetically favored (heat of formation of CuO = −157.3 kJ mol^{-1}) causes further segregation of Cu onto the top layers. The presence of copper oxide on the surface of the Pd nanoparticles could also explain the higher catalytic activity of the bimetallic catalysts. As shown by Dai et al.,[54] copper oxide prevents the aggregation of the palladium nanoparticles. This is clearly what we observed in the HRTEM analysis of the bimetallic sample (see Figure 1 and Figure 3) that gives a narrow distribution of smaller sized nanoparticles.

The catalytic performances of the bimetallic CuPd/PVPy system were herein compared with those obtained by using the corresponding monometallic systems as well as their mixture. The Sonogashira-type carbon–carbon coupling reactions of phenylacetylene with 4-iodotoluene, chosen as model reaction, were carried out in water under air by using low catalyst molar ratio (corresponding to 0.1 mol% of Pd and 0.05 mol%, of Cu, with respect to the iodide; see Figure 8). The CuPd/PVPy system showed a high catalytic activity in the reaction of 4-iodotoluene with phenylacetylene, affording 98% of iodide conversion after 4 h (SA = 167 h^{-1}). On the other hand, under the same reaction conditions the equivalent physical mixture of the monometallic systems (Pd/PVPy + Cu/PVPy) was significantly less active (SA = 43 h^{-1}, 26% conversion after 4 h) and similar results were obtained by using the monometallic Pd/PVPy system (29% conversion after 4 h), whereas the Cu/PVPy monometallic system was almost inactive (less than 3% conversion after 4 h). Catalytic tests carried out under inert atmosphere (i.e. argon) led to comparable results (23.5% of iodide conversion after 1 h, SA = 157 h^{-1}, and 97% conversion after 4 h), proving that air does not affect the catalytic properties of the catalytic system. The substrate scope of the Sonogashira reaction promoted by the CuPd/PVPy was investigated by using different (hetero)aryl iodides containing both electron donating groups as well as electron withdrawing groups (Table 1 S) with aryl acetylenes. In all of the cases, the desired alkyne products were isolated in good to excellent yields (63%–96%).

The higher catalytic efficiency of the bimetallic system compared to that of the corresponding monometallic Pd and Cu systems and of their equivalent physical mixture, shown in Figure 8, suggests that the presence of a Cu–Pd interaction favors a synergic effect between the two metals in Sonogashira reaction, increasing significantly (about 4 times) the activity of the catalyst.

The formation of a Cu oxide shell on the surface of metal Pd nanoparticles could explain this effect. Although the catalytically active species involved in the coupling reaction mechanism are still not well known,[36] it has already been observed that the increase of the catalytic activity in the presence of copper oxide species agrees with the formation of transient Cu-acetylide species which leads to alkynylpalladium(II) derivatives by transmetallation which proceeds to give the required coupled products and to regenerate the active Pd species.[24]

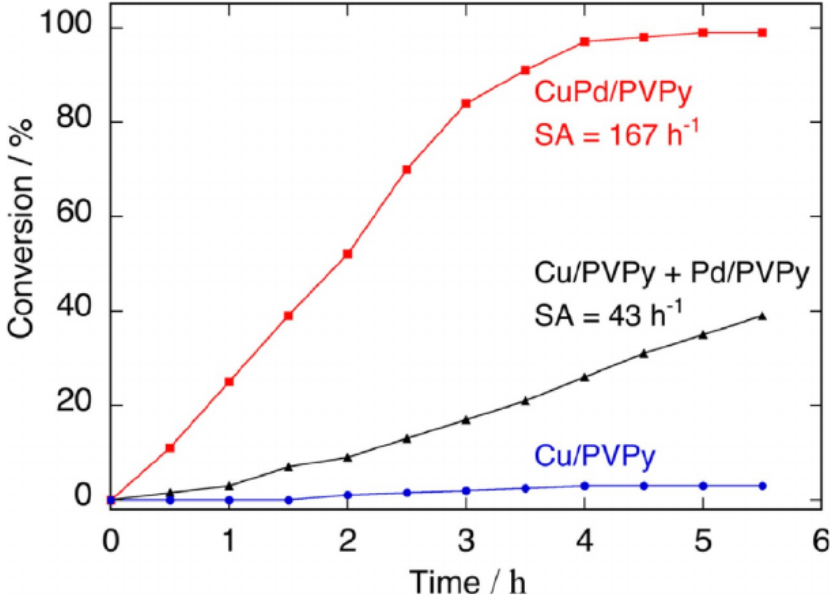

Figure 8. Kinetic study of the Sonogashira reaction between 4-iodotoluene and phenylacetylene catalyzed by CuPd/PVPy, Cu/PVPy, and an equivalent physical mixture of Pd/PVPy and Cu/PVPy systems. Specific activity (SA) was calculated as moles of aryl iodide converted/moles of metal per hour (calculated at about 30% of conversion).

3. Conclusions

A PVPy-supported CuPd bimetallic catalyst was prepared by co-evaporation of Pd and Cu bulk metals, according to MVS synthetic procedure. The system showed higher catalytic efficiency than the analogously prepared Pd and Cu monometallic system and their equivalent mixture in Sonogashira type carbon–carbon coupling reactions of phenylacetylene with 4-iodotoluene carried out in air. Transmission electron microscopy techniques showed the presence of metal Pd nanoparticles distributed in a narrow range (1.0 nm–4.5 nm) with a mean diameter of about 2.5 nm together with the presence of Pd and Cu phases homogeneously distributed within the PVPy support. XAFS analysis allowed to characterize the structure of this system indicating the presence of small metal Pd nanoparticles with some alloying in the immediate subsurface layers with few Cu atoms, whereas a portion of Cu atoms were in an oxidized Cu^{2+} phase probably forming thin and incomplete shells around the Pd-rich cores. The results here reported are an interesting additional example of the strong relation between structural features and catalytic properties in CuPd bimetallic catalysts.

Experimental Section

CuPd Bimetallic Catalyst Preparation

The co-condensation of palladium and copper metals together with mesitylene and 1-hexene solvents was carried out in a static MVS reactor,[55,56] equipped with two alumina-coated tungsten crucibles that allowed evaporating independently the two metals. 150 mg of Pd and 60 mg of Cu were co-condensed with a mixture of 1-hexene (30 mL) and mesitylene (30 mL) under high vacuum (10^{-5} mBar) on the cooled wall (−196 °C) of a glass MVS reactor chamber for one hour. The Cu/Pd nanoparticles solution (24 mL) was added to a mesitylene (20 mL) suspension of the support (4 g) (PVPy, Aldrich product, poly-4-vinylpyridine 2% cross-linked with divinylbenzene, particle size = 60 mesh, $d = 0.45\ g\ m^{-3}$) under argon atmosphere. The mixture was stirred at room (25 °C) temperature for 12 h. Cu/Pd bimetallic nanoparticles were quantitatively deposited on the support, the colorless solution was removed and the solid was washed with *n*-pentane (two portions, 30 mL) and dried under reduced pressure (10^{-3} mBar). A quantitative analysis, performed using inductively coupled plasma optical emission spectrometry (ICP OES, ICAP6300 Duo purchased from Thermo Fisher Scientific) on a CuPd/PVPy sample, after microwave digestion of the samples (ca. 5 mg of catalyst) and dilution with highly deionized water (Milli-Q Academic, Millipore) to a final weight of 100 g, revealed a 1.0 wt.% of Pd and 0.3 wt.% of Cu loading.

CuPd/PVPy-Catalysed Sonogashira Reaction of Phenylacetylene with 4-Iodotoluene

21.2 mg of CuPy/PVPy (2.0×10^{-3} mmol of Pd; 1.0×10^{-3} mmol of Cu), tetrabutylammonium bromide (TBAB, 322 mg, 1.0 mmol), H_2O (5.0 mL), 4-iodotoluene (2.0 mmol), pyrrolidine (4.0 mmol, 284 mg, 334 μL) and phenyl acetylene (2.4 mmol), were added under air atmosphere into a 25 mL round-bottomed, two-necked flask equipped, with a stirring magnetic bar. The reaction mixture was stirred at 95 °C. Samples of the reaction mixture, taken at different times, were cooled to room temperature, and then the organic products were extracted with diethyl ether and dried over anhydrous sodium sulphate. Gas chromatographic (GC) analysis (Agilent Technologies 6890N Network GC system equipped with an Agilent HP-5MS bonded FSOT column (30 m × 0.25 mm, 0.25 μm) was evaluated using calibration curves obtained with naphthalene and an authentic sample of the expected product.

HRTEM and XAFS Characterization

Transmission electron microscopy analysis was performed using a Zeiss LIBRA 200FE analytical transmission electron microscope,

equipped with a STEM facility and EDS probe for chemical analysis. The catalytic samples were deposited on a holey carbon film supported on a copper (or gold for EDS analysis) TEM grid (300 mesh).

The local atomic structure around the Cu atoms was investigated by XAFS spectroscopy measuring the K absorption edge at the Italian GILDA (from 2015 named LISA) beamline[57] of the European Synchrotron Radiation Facility (ESRF, Grenoble, France). The sagittal focusing monochromator was equipped with two Si (311) crystals and used in dynamic focusing mode.[58] All X-ray absorption spectra were collected at liquid nitrogen temperature (LNT) in order to reduce the thermal effects. The reference samples (Cu metallic foil and CuO and Cu_2O oxides) were measured in transmission mode using two Ar-filled ionization chambers to detect the incident (I_0) and transmitted (I_T) X-ray beams. The catalysts at the Cu K-edge were measured in fluorescence mode (I_F) using a 13-element high purity Ge detector coupled to an *x*-ray pulse digital analyzer for a more accurate dead time effect correction.[59] The absorption coefficients were calculated as $\mu(E)=\ln(I_0/I_T)$ in transmission mode and as $\mu(E)=(I_F/I_0)$ in fluorescence mode. The XAFS catalytic samples were prepared mixing their fine powders with boron-nitride and pressing them into pellets. The different sample amounts were calculated[60] in order to achieve appropriate edge jumps. The XAFS measurements of the reference samples were used to calibrate the energy scales, to align the absorption spectra and to evaluate the S_0^2 values.[61] The structural characterization was performed taking into account the near edge structure (XANES) part of the XAFS spectra and the extended X-ray absorption fine structure (EXAFS) data.

In particular the MXAN program, that applies the extended continuum multiple scattering (ECMS) theory[51] to the first 200 eV of *x*-ray absorption spectra, was used to perform a quantitative analysis, including interatomic distances and angles, in the fitting procedure of the CuPd XANES spectrum at the Cu K-edge. The MXAN fitting procedure followed an iterative approach fitting one site but including the contribution to the total absorption cross-section of the second site whose local geometry was kept fixed.[62] The two sites were combined in each fitting procedure with a 0.5 weight. In the first step one site was refined while the other was held constant; in the second step the second site was refined but the fitting procedure included for the first site the best fit geometrical conditions previously achieved and so on. The fitting procedures the two sites where continuously and separately optimized until a reasonable convergence was reached.

The EXAFS data or $\chi(k)$, given by the normalized oscillations superimposed onto the measured absorption coefficient $\mu(E)$ are defined as $\chi(k)=[\mu(k)-\mu_0(k)]/\mu_0(k)$, where $\mu_0(k)$ is the total atomic absorption coefficient and $k=[2\,m(E-E_0)/\hbar^2]^{1/2}$ is the photoelectron wave vector given, where E is the incoming photon energy and E_0 is the threshold energy that is determined as the inflection point of the measured absorption edge. The EXAFS data were extracted using the ATHENA program[63] and the least-squares parameter fitting was performed using the ARTEMIS program,[63] both implemented in the IFEFFIT package.[64] The k^2-weighted EXAFS data were Fourier transformed using a Hanning window over a *k*-range (2.7–12.2) $Å^{-1}$. Data fitting was performed in R-space but the fitting procedure was also verified in the back transformed k-space. EXAFS data analysis was used to determine the coordination numbers, N, interatomic distances, R, and Debye–Waller factors, σ^2, of the coordination shells around the central absorbing Cu atoms. An estimation of the accuracy of the obtained structural parameters, compatible with the data quality and k-range used[65] was achieved. In the fitting procedure of the reference samples the coordination numbers were fixed to the values of their corresponding crystallographic structures and single and multiple-scattering contributions, calculated using the FEFF6 software package,[66] were used. The fitting procedure of the EXAFS data of the CuPd catalyst was based only on single scattering.

Acknowledgements

This work was partially supported by the Italian Ministry of University and Scientific Research (MIUR) under the FIRB 2010 program (RBFR10BF5V).

Conflict of interest

The authors declare no conflict of interest.

Keywords: bimetallic CuPd catalyst · transmission electron microscopy · metal vapor synthesis · Sonogashira reactions · XAFS spectroscopy

[1] N. Toshima, H. Yan, Y. Shiraishi, B. Corain, *Metal Nanoclusters in Catalysis and Materials Science. The Issue of Size-Control*, (Eds.: G. Schmid, N. Toshima), Elsevier, Amsterdam, **2008**, pp. 49 – 75.
[2] J. Ferrando, J. Jellinek, R. L. Johnston, *Chem. Rev.* **2008**, *108*, 845 – 910.
[3] L. Guczi, *Catal. Today* **2005**, *101*, 53 – 64 and references therein.
[4] A. Kulkarni, B. C. Gates, *Angew. Chem. Int. Ed.* **2009**, *48*, 9697 – 9700; *Angew. Chem.* **2009**, *121*, 9877 – 9880.
[5] CK. Sun, J. Liu, N. K. Nag, N. D. Browning, *J. Phys. Chem. B* **2002**, *106*, 12239 – 12246.
[6] O. M. Ilinitch, F. P. Cuperus, L. V. Nosova, E. N. Gribov, *Catal. Today* **2000**, *56*, 137 – 145.
[7] B. Coq, F. Figueras, *J. Mol. Catal. A* **2001**, *173*, 117 – 134.
[8] L. Zhu, K. S. L. B. Zhang, J. S. Bradley, A. E. De Pristo, *J. Catal.* **1997**, *167*, 412 – 416.
[9] J. Trawczyński, P. Gheeka, J. Okalb, M. Zawadzkib, M. J. Ilan Gomezc, *Appl. Catal. A* **2011**, *409 – 410*, 39 – 47.
[10] K. A. Guy, H. Xu, J. C. Yang, C. J. Werth, J. R. Shapley, *J. Phys. Chem. C* **2009**, *113*, 8177 – 8185.
[11] S. Chen, H. Zhang, L. Wu, Y. Zhao, C. Huang, M. Ge, Z. Liu, *J. Mater. Chem.* **2012**, *22*, 9117 – 9122.
[12] J. Müslehiddinoğlu, J. Li, S. Tummala, R. Deshpande, *Org. Process Res. Dev.* **2010**, *14*, 890 – 894.
[13] K. I. Choi, M. A. Vannice, *J. Catal.* **1991**, *131*, 36 – 50.
[14] R. Brayner, D. dos Santos Cunha, F. Bozon-Verduraz, *Catal. Today* **2003**, *78*, 419 – 432.
[15] S. R. Chowdhury, P. Mukherjee, S. K. Bhattachrya, *Int. J. Hydrogen Energy* **2016**, *41*, 17072 – 17083.
[16] F. Illas, N. Lopez, J. M. Ricart, A. Clotet, J. C. Conesa, M. Fernandez-Garcia, *J. Phys. Chem. B* **1998**, *102*, 8017 – 8023.
[17] S. V. Myers, A. I. Frenkel, R. M. Crooks, *Chem. Mater.* **2009**, *21*, 4824 – 4829.
[18] W. Shi, X. Chen, S. Xu, J. Cui, L. Wang, *Nano Res.* **2016**, *9*, 2912 – 2920.
[19] F. Heshmatpour, R. Abazari, S. Balalaie, *Tetrahedron* **2012**, *68*, 3001 – 3011.
[20] C. Rossy, E. Fouquet, F.-X. Felpin, *Beilstein J. Org. Chem.* **2013**, *9*, 1426 – 1431.
[21] R. Cano, M. Yus, D. J. Ramon, *Tetrahedron* **2012**, *68*, 1393 – 1400.
[22] T. V. Magdesieva, O. M. Nikitin, A. V. Yakimansky, M. Ya Goikhman, I. V. Podeshvo, *Electrochim. Acta* **2011**, *56*, 3666 – 3672.
[23] S. Chouzier, M. Gruber, L. Djakovitch, *J. Mol. Catal. A* **2004**, *212*, 43 – 52.
[24] D. Sengupta, J. Saha, G. De, B. Basu, *J. Mater. Chem. A* **2014**, *2*, 3986 – 3992.
[25] M. Korzec, P. Bartczak, A. Niemczyk, J. Szade, M. Kapkowski, P. Zenderowska, K. Balin, J. Lelatko, J. Polanski, *J. Catal.* **2014**, *313*, 1 – 8.
[26] M. Gholinejad, N. Jeddi, B. Pullithadathil, *Tetrahedron* **2016**, *72*, 2491.

[27] S. Diyarbakir, H. Can, Ö. Metin, *ACS Appl. Mater. Interfaces* **2015**, *7*, 3199.
[28] W. Xu, H. Sun, B. Yu, G. Zhang, W. Zhang, Z. Gao, *ACS Appl. Mater. Interfaces* **2014**, *6*, 20261.
[29] M. Gholinejad, J. Ahmadi, *ChemPlusChem* **2015**, *80*, 973.
[30] C. Rossy, J. Majimel, M. Tréguer Delapierre, E. Fouquet, F.-X. Felpin, *J. Organomet. Chem.* **2014**, *755*, 78.
[31] M. Gholinejad, J. Ahmadi, C. Nájera, M. Seyedhamzeh, F. Zareh, M. Kompany-Zareh, *ChemCatChem* **2017**, *9*, 1442 – 1449.
[32] R. Chinchilla, C. Nájera, *Chem. Soc. Rev.* **2011**, *40*, 5084 – 5121.
[33] K. C. Nicolaou, P. G. Bulger, D. Sarlah, *Angew. Chem. Int. Ed.* **2005**, *44*, 4442 – 4489; *Angew. Chem.* **2005**, *117*, 4516 – 4563.
[34] U. H. F. Bunz, *Chem. Rev.* **2000**, *100*, 1605 – 1644.
[35] K. Onitsuka, M. Fujimoto, N. Ohshiro, S. Takahashi, *Angew. Chem. Int. Ed.* **1999**, *38*, 689 – 692; *Angew. Chem.* **1999**, *111*, 751 – 754.
[36] K. Sonogashira, *J. Organomet. Chem.* **2002**, *653*, 46 – 49.
[37] C. Evangelisti, N. Panziera, P. Pertici, G. Vitulli, P. Salvadori, C. Battocchio, G. Polzonetti, *J. Catal.* **2009**, *262*, 287 – 293.
[38] A. Balerna, C. Evangelisti, R. Psaro, G. Fusini, A. Carpita, *J. Phys. Conf. Ser.* **2016**, *712*, 012057.
[39] A. F. Lee, P. J. Ellis, I. J. S. Fairlam, K. Wilsona, *Dalton Trans.* **2010**, *39*, 10473.
[40] W. Oberhauser, C. Evangelisti, R. P. Jumde, G. Petrucci, M. Bartoli, M. Frediani, M. Mannini, L. Capozzoli, E. Passaglia, L. Rosi, *J. Catal.* **2015**, *330*, 187 – 196.
[41] A. Balerna, C. Evangelisti, C. Tiozzo, *X-Ray Spectrom.* **2017**, https://doi.org/10.1002/xrs.2731.
[42] P. Abdulkin, Y. Moglie, B. R. Knappett, D. A. Jefferson, M. Yus, F. Alonso, A. E. H. Wheatley, *Nanoscale* **2013**, *5*, 342.
[43] J. M. Tranquada, S. M. Heald, A. R. Moodenbaugh, *Phys. Rev. B* **1987**, *36*, 5263.
[44] J. Y. Kim, J. A. Rodriguez, J. C. Hanson, A. I. Frenkel, P. L. Lee, *J. Am. Chem. Soc.* **2003**, *125*, 10684.
[45] A. Kuzmin, A. Anspoks, A. Kalinko, A. Rumjancevs, J. Timoshenko, L. Nataf, F. Baudelet, T. Irifune, *Physics Procedia* **2016**, *85*, 27 – 35.
[46] D. G. Nicholson, M. H. Nilsen, *J. Mater. Chem.* **2000**, *10*, 1965.
[47] J. Garcia, M. Benfatto, C. R. Natoli, A. Bianconi, A. Fontaine, H. Tolentino, *Chem. Phys.* **1989**, *132*, 295.
[48] L. Palladino, S. Della Longa, A. Reale, M. Belli, A. Scafati, G. Onori, A. Santucci, *J. Chem. Phys.* **1993**, *98*, 2720.
[49] A. I. Frenkel, G. V. Korshin, *Canadian Journal of Soil Science* **2001**, *81*, 271.
[50] S. W. T. Price, J. D. Speed, P. Kannan, A. E. Russell, *J. Am. Chem. Soc.* **2011**, *133*, 19448.
[51] M. Benfatto, S. Della Longa, *J. Synchrotron Radiat.* **2001**, *8*, 1087 – 1094.
[52] B. J. Hathaway, D. E. Billing, *Coord. Chem. Rev.* **1970**, *5*, 143.
[53] G. Mattei, C. Maurizio, P. Mazzoldi, F. D'Acapito, G. Battaglin, E. Cattaruzza, C. de Julián Fernández, C. Sada, *Phys. Rev. B* **2005**, *71*, 195418.
[54] C. Dai, X. Li, A. Zhang, C. Liu, C. Songabc, X. Guo, *RSC Adv.* **2015**, *5*, 40297.
[55] C. Evangelisti, E. Schiavi, L. A. Aronica, A. M. Caporusso, G. Vitulli, L. Bertinetti, G. Martra, A. Balerna, S. Mobilio, *J. Catal.* **2012**, *286*, 224 – 236.
[56] L. A. Aronica, A. M. Caporusso, G. Tuci, C. Evangelisti, M. Manzoli, M. Botavina, G. Martra, *Appl. Catal. A* **2014**, *480*, 1 – 9.
[57] a) S. Pascarelli, F. D'Acapito, G. Antonioli, A. Balerna, F. Boscherini, R. Cimino, G. Dalba, P. Fornasini, G. Licheri, C. Meneghini, F. Rocca, S. Mobilio, *ESRF Newslett.* **1995**, *23*, 17; b) F. d'Acapito, A. Trapananti, A. Puri, *J. Phys. Conf. Ser.* **2016**, *712*, 012021.
[58] S. Pascarelli, F. Boscherini, F. D'Acapito, J. Hrdy, C. Meneghini, S. Mobilio, *J. Synchrotron Radiat.* **1996**, *3*, 147 – 155.
[59] G. Ciatto, F. d'Acapito, F. Boscherini, S. Mobilio, *J. Synchrotron Radiat.* **2004**, *11*, 278 – 283.
[60] P. A. Lee, P. H. Citrin, P. Eisenberger, B. M. Kincaid, *Rev. Mod. Phys.* **1981**, *53*, 769.
[61] J. J. Rehr, R. C. Albers, *Rev. Mod. Phys.* **2000**, *72*, 621.
[62] P. Frank, M. Benfatto, M. Qayyam, B. Hedman, K. O. Hodgson, *J. Chem. Phys.* **2015**, *142*, 084310.
[63] B. Ravel, M. Newville, *J. Synchrotron Radiat.* **2005**, *12*, 537.
[64] M. Newville, *J. Synchrotron Radiat.* **2001**, *8*, 322.
[65] G. G. Li, F. Bridges, C. H. Booth, *Phys. Rev. B* **1995**, *52*, 6332.
[66] S. I. Zabinsky, J. J. Rehr, A. Ankudinov, R. C. Albers, M. J. Eller, *Phys. Rev. B* **1995**, *52*, 2995 – 3009.